COMMUNICATION

Monodisperse SnSb nanocrystals for Li-ion and Na-ion battery anodes: synergy and dissonance between Sn and Sb†

Meng He,‡[a,b] Marc Walter,‡[a,b] Kostiantyn V. Kravchyk,‡[a,b] Rolf Erni,[c] Roland Widmer[d] and Maksym V. Kovalenko*[a,b]

We report a facile chemical synthesis of monodisperse colloidal SnSb nanocrystals (NCs) *via* reaction between Sn NCs and SbCl₃ in oleylamine under reducing conditions. In comparison with individual Sn and Sb NCs and their mixtures, we show that through the creation of SnSb alloyed NCs the Li-ion storage properties are enhanced due to combination of high cycling stability of Sb with higher specific Li-ion storage capacity of Sn. In particular, stable capacities of above 700 and 600 mA h g⁻¹ were obtained after 100 cycles of charging/discharging at 0.5C and 4C rates, respectively (1C corresponding to a current density of 660 mA g⁻¹). Furthermore, Na-ion storage capacities of >350 mA h g⁻¹ and >200 mA h g⁻¹ were obtained at 1C and 20C rates, respectively. This study highlights the differences between Li- and Na-ion (electro)chemistries and the great utility of monodisperse NCs as model systems for understanding size and compositional effects on the performance of conversion-type electrode materials.

Monodisperse inorganic nanocrystals (NCs) and nanoparticles (NPs) can serve as well-defined model systems for controlling and studying the effects of the primary particle size, composition and morphology of electrode materials on their reversible electrochemical cycling in Li-ion batteries (LIBs) and in emerging, analogous Na-ion battery technology (SIBs). Particularly interesting are NCs and NPs of anode materials which operate *via* alloying with either Li (Si, Sn, Sb, Ge) or Na (Sn, Sb, P).[1–4] These alloys (*e.g.* Li_3Sb, Na_3Sb, $Li_{22}Si_5$ *etc.*) provide theoretical charge storage capacities 2–10 higher than that of

[a]ETH Zürich – Swiss Federal Institute of Technology Zürich, Vladimir Prelog Weg 1, CH-8093 Zürich, Switzerland. E-mail: mvkovalenko@ethz.ch
[b]Empa-Swiss Federal Laboratories for Materials Science and Technology, Laboratory for Thin Films and Photovoltaics, CH-8600 Dübendorf, Switzerland
[c]Electron Microscopy Center, Empa – Swiss Federal Laboratories for Materials Science and Technology, CH-8600 Dübendorf, Switzerland
[d]Nanotech@surfaces Laboratory, Empa – Swiss Federal Laboratories for Materials Science and Technology, CH-8600 Dübendorf, Switzerland
†Electronic supplementary information (ESI) available: Materials and methods, additional structural and electrochemical characterization. See DOI: 10.1039/c4nr05604c
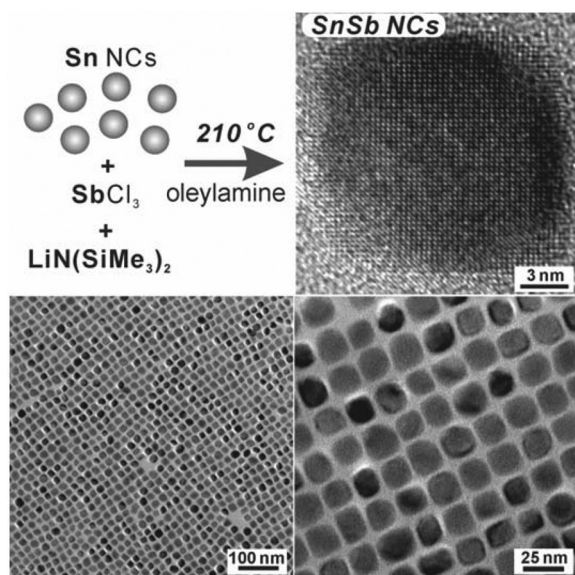‡These authors contributed equally.

commercially used graphite anodes (372 mA h g⁻¹ for LiC_6). Notably, graphite stores negligible amounts of Na-ions, indicating an urgent need for research towards stable Na-ion anode materials. All aforementioned alloying materials undergo massive volume changes by 100–400% upon full lithiation or sodiation, leading to mechanical destruction of the electrodes. Downsizing of the active material primary size to nanoscopic forms is presently studied as a major approach for mitigating the effects of the volume changes and to enhance the reaction kinetics.[5–8] In this regard, we recently demonstrated the clear size-dependence of both the cycling stability and rate capability by using precisely engineered, 10–20 nm large NCs of Sn[9] and Sb[10] as Li- and Na-ion storage media.

The following questions had triggered this study: can one further tailor the electrochemical properties by combining two or more active materials in a well-controlled fashion, that is, using pre-engineered monodisperse NCs? Will this combined effect be an enhancement over individual properties of nanoscopic Sn and Sb, an average of two, or deterioration? Furthermore, Li-ion and Na-ion electrochemistries of the same electrode material are often considerably different.[11,12] We therefore thought to study Li-ion and Na-ion storage properties of monodisperse SnSb NCs and compare the results with individual Sn and Sb NCs and their mixtures. Although there have been several previous studies on SnSb electrodes for LIBs and SIBs,[13–22] the questions raised here require obtaining Sn, Sb and SnSb in the form of uniform colloidal NCs of very similar size. In the following, we present a facile colloidal synthesis of monodisperse SnSb NCs. Then we show that Li-ion storage properties of SnSb NCs are significantly enhanced as compared to individual Sn, Sb NCs and their mixtures, both in terms of charge storage capacity and cycling stability. As a result, high charge storage capacities above 700 and 600 mA h g⁻¹ were obtained after 100 cycles of charging/discharging at 0.5C and 4C rates, respectively (1C corresponding to a current density of 660 mA g⁻¹). In Na-ion cells, in contrast, we find that the presence of Sn reduces the overall Na-ion storage

Fig. 1 (A) Schematics of one-pot synthesis of SnSb NCs, along with high- and low-resolution transmission electron microscopy (TEM) images of ~20 nm SnSb NCs.

capacity to *ca.* 350 mA h g^{-1} and 200 mA h g^{-1} at 1C and 20C rates, respectively, while maintaining high cycling stability and high rate capability.

SnSb NCs were obtained *via* a successive reduction of the respective Sn and Sb precursor in one-pot synthesis (Fig. 1, for details, see ESI†). First, Sn NC seeds were synthesized according to our previously reported procedure.[9] Ten seconds after the nucleation of Sn NCs, the Sb precursor was injected into the hot solution at 210 °C. Within several minutes Sn–Sb alloy was formed, as can be illustrated by XRD patterns (Fig. 2), and after ripening for several hours uniform ~20 nm SnSb NCs with narrow size distribution (<10%, Fig. S1 and S2 of ESI†) were obtained. In this reaction, inexpensive tin(II) and
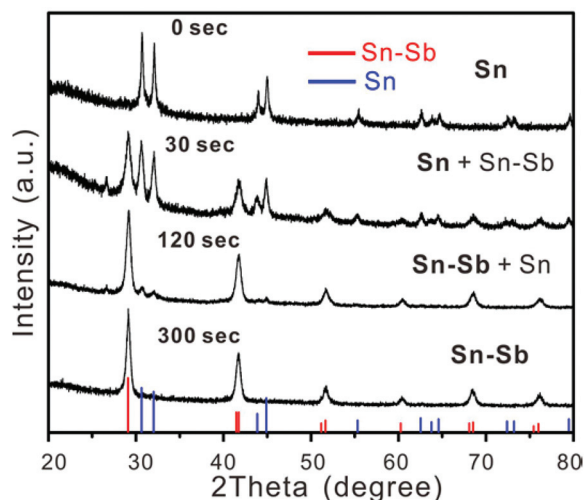

Fig. 2 Evolution of powder X-ray diffraction (XRD) patterns during the conversion of Sn NCs into SnSb NCs.

antimony(III) chlorides are used as precursors, while lithium bistrimethylsilylamide [LiN(SiMe$_3$)$_2$] serves as a mild base for partial deprotonation of oleylamine according to the acid–base equilibrium: R-NH$_2$ + LiN(SiMe$_3$)$_2$ ↔ R-NHLi + HN(SiMe$_3$)$_2$. The Sn/Sb-oleylamide species are then formed *in situ via* the reaction of Li-oleylamide with Sn(II)/Sb(III) chlorides,[9,10] and serve as the actual precursors being reduced (Sn) or thermally decomposed (Sb). It should be pointed out that the simultaneous injection of Sn and Sb chlorides leads only to the formation of Sb NCs (Fig. S3A of ESI†) due to the higher reactivity (instability) of the Sb precursor. Equally important is not to age Sn seeds for too long before adding the Sb precursor, as this may lead to a mixture of Sn and SnSb phases (Fig. S3B†). High-resolution TEM images (Fig. 1) demonstrate the crystallinity of SnSb NCs. Elemental mapping with energy dispersive X-ray spectroscopy in scanning TEM mode (EDX-STEM) suggest uniform alloying (Fig. S4†). Rietveld refinement of XRD patterns (Fig. S5†) matches the known rhombohedral crystal structure of β-SnSb.[23] β-SnSb has essentially a cubic NaCl-type structure with a slight rhombohedral distortion (a_{rho} ~ 6.13 Å, α ~ 89.6°). This can explain the propensity to form cubic or truncated cubic NCs. The Sn : Sb atomic ratio was 3 : 2, as estimated by EDX analysis and verified by inductively coupled plasma-optical emission spectrometry (ICP-OES; Table S1†). This composition is in good agreement with the reported homogeneity region of ±10 at% in β-SnSb.[23,24]

Before testing the performance of SnSb NCs as anode materials in LIBs and SIBs, the insulating long-chain capping ligands were removed by treating with a 1 M solution of hydrazine in acetonitrile, a method commonly used for improving charge transport in quantum dot solids[25–27] and previously used for Sn, Sb and SnGe NC anodes.[9,10,28] All electrodes were tested under the same conditions in coin-type half-cells with metallic Li or Na as counter electrodes. Working electrodes contained 64 wt% of the active material, carboxymethylcellulose (CMC, 15 wt%) as a polymer binder, and amorphous carbon as a conductive additive (21%). The films were cast from aqueous slurries and after vacuum drying had a similar mass loading of ~0.5 mg cm^{-2}. Fluoroethylenecarbonate (FEC) was used as the electrolyte additive for stabilizing the solid-electrolyte interface (SEI).[8]

SnSb NCs as LIB anodes

So far, very few reports have dealt with micro- and nanoscopic SnSb powders as anode materials in LIBs.[13–19,22] The best performances were characterized by the capacities of up to 500–600 mA h g^{-1} (0.2C rate), obtained for mechanochemically synthesized nanocomposites of SnSb with carbon.[19,22]

Fig. 3A compares the capacities and cycling stabilities obtained for SnSb NCs and, for comparison, for individual Sn and Sb NCs and their mixtures. Owing to the SEI formation and reduction of surface oxides (see Fig. S11† for XPS spectra), coulombic efficiencies of 40–50% were obtained for the first cycle, but approached 97–99% during subsequent cycling.
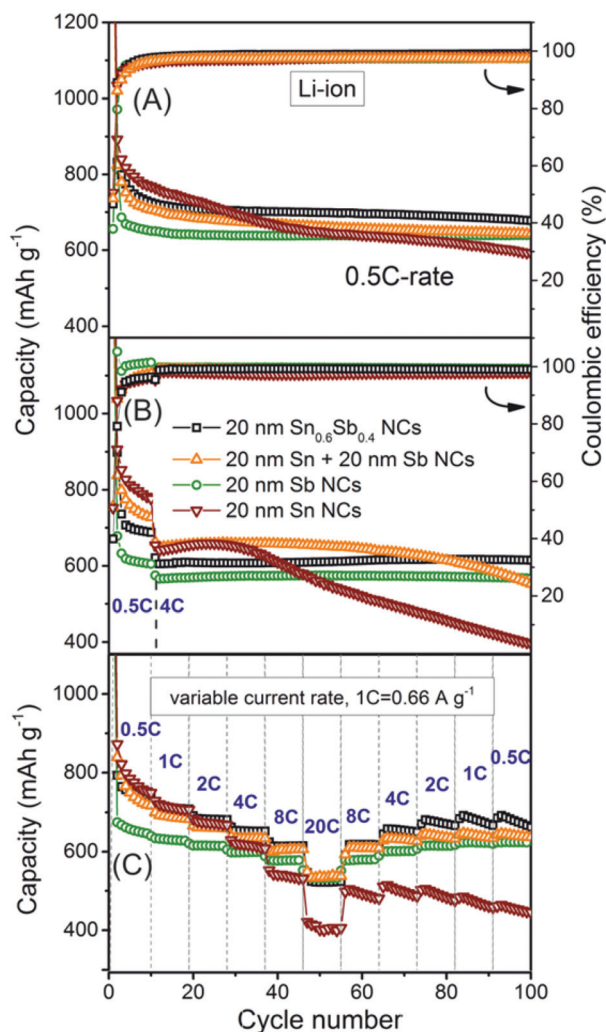
Fig. 3 (A, B) Galvanostatic cycling stability tests at current densities of 0.33 A g^{-1} and 2.64 A g^{-1}, and (C) rate capability tests (0.5–20C rates, 1C = 660 mA g^{-1} based on the theoretical capacity of pure Sb) for Li-ion anodes composed of SnSb, Sn and Sb NCs. The first two cycles for all electrodes shown in (B, C) were carried out at 0.1C rate. All batteries were cycled in the voltage window of 0.02–1.5 V.

In accordance with the higher theoretical capacity of Sn (992 mA h g^{-1}) *vs.* Sb (660 mA h g^{-1}), all Sn-containing electrodes showed higher initial capacities than pure Sb NCs. At the same time, pure Sn NCs showed the lowest cycling stability. Alloying with Sb allowed combining the excellent cycling stability and the rate capability of Sb (see Fig. 3 and ref. 10) with the higher capacity of Sn. The high cycling stability and rate capability of Sb have been previously ascribed[10,29] to smaller volumetric expansion upon full lithiation (ΔV = 135%), a fewer number of intermediate crystalline phases during cycling (only one – Li$_2$Sb), as compared to Sn (ΔV = 300%, 7 crystalline Li–Sn alloys),[3] and faster Li-ion diffusion in the layered structure of Sb. Importantly, at a higher current density of 2.64 A g^{-1} (4C rate) alloyed SnSb NCs possess much higher cycling stability than the mechanical mixtures of Sn and Sb NCs of the same size (Fig. 3B). Capacities of at least 700 and 600 mA h g^{-1} can
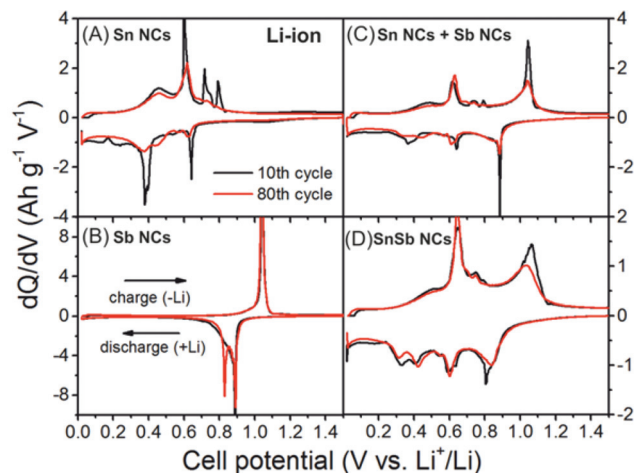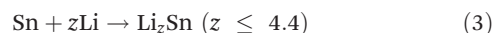

Fig. 4 Differential capacity plots obtained from galvanostatic discharge/charge curves during 10th and 80th cycles at a current density of 0.33 A g^{-1}.

be obtained after 100 cycles of charging/discharging at 0.5C and 4C rates. Important hints into the origin of this difference are provided by differential capacity plots (dQ/dV), shown for the 10th and 80th cycles (Fig. 4A and S6†), and by cyclic voltammograms (CVs, Fig. S6†). For both SnSb nanoalloys and Sb/Sn NC mixtures, dQ/dV plots and CVs are the sum of the curves obtained for Sn and Sb NCs. This is in agreement with previous *in situ* XRD studies showing that lithiation of SnSb produces crystalline Li$_3$Sb and amorphous Li$_z$Sn alloys:[21,30,31]

$$SnSb + xLi \rightarrow Li_xSnSb \quad (1)$$

$$Li_xSnSb + yLi \rightarrow Li_{x+y}Sn_{1-m}Sb + mSn \leftrightarrow Li_3Sb + Sn \quad (2)$$

$$Sn + zLi \rightarrow Li_zSn \ (z \leq 4.4) \quad (3)$$

However, compared to the bulk material dQ/dV peaks for SnSb nanoalloys are much broader. Such broadening is often attributed to their very small crystallite size during the cycling, since at the nanoscale the electrochemical reactions are known to occur within much broader voltage intervals. Accordingly, the superior cycling stability of SnSb nanoalloys can be explained by much smaller mean crystallite size during the electrochemical cycling.

SnSb NCs as Na-ion anode materials

The search for efficient anode materials for SIBs is critically important because well-studied Li-ion anode materials such as graphite or silicon show uptake of only negligible amounts of Na-ions.[32,33] In the first cycle, Na-ion charge storage capacities of SnSb NCs were 360–370 mA h g^{-1} at 0.5C rate (Fig. 5A). Upon subsequent cycling at 1C and 20C rates, stable capacities of 350 mA h g^{-1} and 230 mA h g^{-1}, respectively, were maintained for more than 100 cycles. Rate-capability tests at 0.5–20C rate showed full capacity recovery, or even higher capacities after the moderate cycling rate of 0.5C is resumed
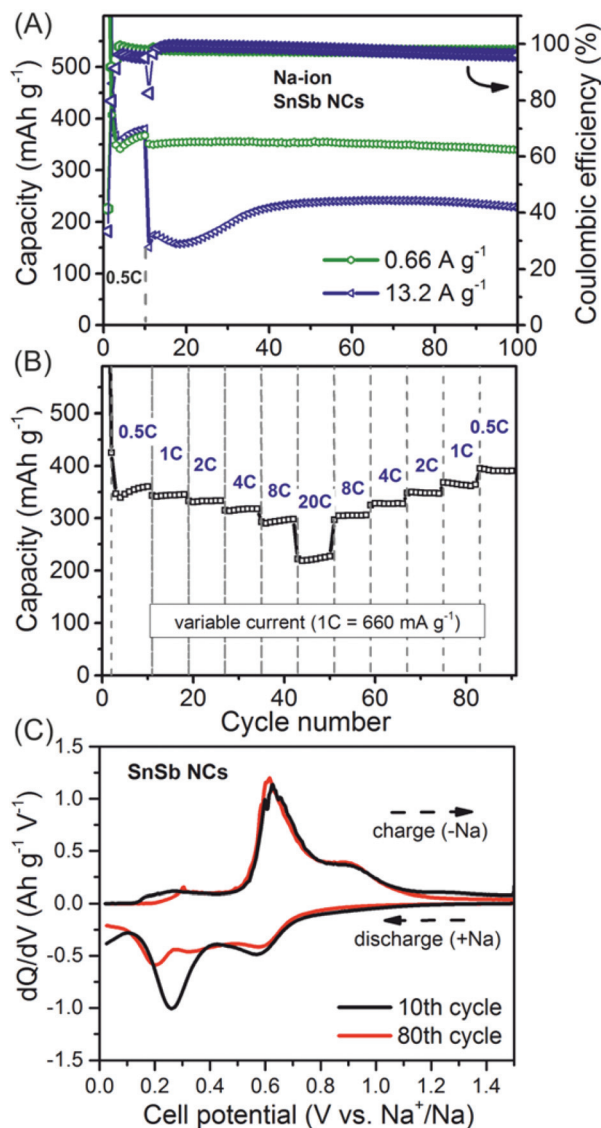
Fig. 5 (A) Galvanostatic cycling stability tests at 1C and 20C rates, and (B) rate capability tests (0.5–20C rates, 1C = 660 mA g^{-1}) for Na-ion anodes comprising SnSb NCs as the storage material. The first two cycles for all electrodes shown in (A, B) were carried out at 0.1C rate. (C) Differential capacitance plots corresponding to the 10th and 80th cycles at 1C rate. All batteries were cycled at voltages of 0.02–1.5 V.

(Fig. 5B). To our knowledge, this is the first study showing high rate-capability and stability at high current rates in SnSb anodes. Coulombic efficiencies were 97–98% (higher for 0.5C rates), still indicating the suboptimal stability of the SEI layer.

Should there be full sodiation to Na$_3$Sb (660 mA h g^{-1}) and Na$_{15}$Sn$_4$ (847 mA h g^{-1}), the capacity of SnSb NCs must reach 750 mA h g^{-1}. Instead, our results and three recent reports[20,21,34] show similar capacities of 300–400 mA h g^{-1} at 0.2–1C rates. This is where the difference between Li and Na-ion insertion chemistries may come into play. While the performance of SnSb electrodes in LIBs can be considered as addition of Sn and Sb vs. Li., plus the stabilizing effect of nanosizing and of atomic intermixing, the alloying chemistry

of SnSb-based SIB anodes is clearly different from pure Sn and Sb. This can be clearly seen from dQ/dV plots and CVs (Fig. 5A and S7†). Recent *in situ* XRD studies of Darwiche *et al.*[21] have shown that sodiation and desodiation of SnSb lead to products without resolvable XRD peaks, consistent with very broad electrochemical features. We also hypothesize that in the SnSb composite the sodiation of Sn is incomplete, as it extends below 0.02 V *vs.* Li. dQ/dV plots and CV of Sn NC electrodes showed that more than 50% of Na-ions are inserted at very low potentials and sodiation is at the steepest rise at 0.02 V (Fig. S7†), with a stable capacity of 350 mA h g^{-1} maintained for 100 cycles at 0.2C rate (Fig. S8†). A large volume change ($\Delta V = 420\%$ for the Sn $\rightarrow$ Na$_{15}$Sn$_4$ transition), lower voltage of alloying and slower diffusion of Na-ions lead to incomplete sodiation and far poorer cycling of Sn *vs.* Na than *vs.* Li.[35,36]

In summary, we report a facile colloidal synthesis of alloyed SnSb NCs. In comparison with individual Sn and Sb NCs, we show that through the creation of SnSb alloyed NCs the Li-ion storage properties are enhanced due to combination of the high cycling stability of Sb with the higher specific Li-ion storage capacity of Sn. In particular, stable capacities of above 700 and 600 mA h g^{-1} were obtained after 100 cycles of charging/discharging at 0.5C and 4C rates. Furthermore, Na-ion storage capacities of >350 mA h g^{-1} and >200 mA h g^{-1} were obtained at 1C and 20C rates, respectively. In Na-ion anodes, mainly the Na$_x$Sb phase is formed, whereas Sn contributes only a marginal capacity. This study points to the important differences between Na- and Li-ion chemistries and to the advantages provided by monodisperse NCs for understanding electrochemical properties of nanoscopic electrode materials.

Acknowledgements

Notes and references

1 C. M. Hayner, X. Zhao and H. H. Kung, *Annu. Rev. Chem. Biomol. Eng.*, 2012, **3**, 445–471.

2 V. Palomares, M. Casas-Cabanas, E. Castillo-Martínez, M. H. Han and T. Rojo, *Energy Environ. Sci.*, 2013, **6**, 2312–2337.

3 C.-M. Park, J.-H. Kim, H. Kim and H.-J. Sohn, *Chem. Soc. Rev.*, 2010, **39**, 3115–3141.

4 Y. Kim, Y. Park, A. Choi, N. S. Choi, J. Kim, J. Lee, J. H. Ryu, S. M. Oh and K. T. Lee, *Adv. Mater.*, 2013, **25**, 3045–3049.

5 C. K. Chan, H. Peng, G. Liu, K. McIlwrath, X. F. Zhang, R. A. Huggins and Y. Cui, *Nat. Nanotechnol.*, 2008, **3**, 31–35.

6 A. Magasinski, P. Dixon, B. Hertzberg, A. Kvit, J. Ayala and G. Yushin, *Nat. Mater.*, 2010, **9**, 353–358.

7 I. Kovalenko, B. Zdyrko, A. Magasinski, B. Hertzberg, Z. Milicev, R. Burtovyy, I. Luzinov and G. Yushin, *Science*, 2011, **334**, 75–79.

8 A. M. Chockla, K. C. Klavetter, C. B. Mullins and B. A. Korgel, *Chem. Mater.*, 2012, **24**, 3738–3745.

9 K. Kravchyk, L. Protesescu, M. I. Bodnarchuk, F. Krumeich, M. Yarema, M. Walter, C. Guntlin and M. V. Kovalenko, *J. Am. Chem. Soc.*, 2013, **135**, 4199–4202.

10 M. He, K. Kravchyk, M. Walter and M. V. Kovalenko, *Nano Lett.*, 2014, 1255–1262.

11 S.-W. Kim, D.-H. Seo, X. Ma, G. Ceder and K. Kang, *Adv. Energy Mater.*, 2012, **2**, 710–721.

12 S. Y. Hong, Y. Kim, Y. Park, A. Choi, N.-S. Choi and K. T. Lee, *Energy Environ. Sci.*, 2013, **6**, 2067–2081.

13 L. Shi, H. Li, Z. Wang, X. Huang and L. Chen, *J. Mater. Chem.*, 2001, **11**, 1502–1505.

14 S. A. Needham, G. X. Wang and H. K. Liu, *J. Alloys Compd.*, 2005, **400**, 234–238.

15 G. Zhang, K. Huang, S. Liu, W. Zhang and B. Gong, *J. Alloys Compd.*, 2006, **426**, 432–437.

16 H. Zhao, C. Yin, H. Guo and W. Qiu, *Electrochem. Solid-State Lett.*, 2006, **9**, A281.

17 C. M. Park and K. J. Jeon, *Chem. Commun.*, 2011, **47**, 2122–2124.

18 J. Li, Q. Ru, S. Hu, D. Sun, B. Zhang and X. Hou, *Electrochim. Acta*, 2013, **113**, 505–513.

19 J.-U. Seo and C.-M. Park, *J. Mater. Chem. A*, 2013, **1**, 15316.

20 L. Xiao, Y. Cao, J. Xiao, W. Wang, L. Kovarik, Z. Nie and J. Liu, *Chem. Commun.*, 2012, **48**, 3321–3323.

21 A. Darwiche, M. T. Sougrati, B. Fraisse, L. Stievano and L. Monconduit, *Electrochem. Commun.*, 2013, **32**, 18–21.

22 C.-M. Park and H.-J. Sohn, *Electrochim. Acta*, 2009, **54**, 6367–6373.

23 L. Norén, R. L. Withers, S. Schmid, F. J. Brink and V. Ting, *J. Solid State Chem.*, 2006, **179**, 404–412.

24 V. Vassiliev, M. Lelaurain and J. Hertz, *J. Alloys Compd.*, 1997, **247**, 223–233.

25 M. Law, J. M. Luther, Q. Song, B. K. Hughes, C. L. Perkins and A. J. Nozik, *J. Am. Chem. Soc.*, 2008, **130**, 5974–5985.

26 D. V. Talapin and C. B. Murray, *Science*, 2005, **310**, 86–89.

27 H. Zhang, B. Hu, L. Sun, R. Hovden, F. W. Wise, D. A. Muller and R. D. Robinson, *Nano Lett.*, 2011, **11**, 5356–5361.

28 M. I. Bodnarchuk, K. V. Kravchyk, F. Krumeich, S. Wang and M. V. Kovalenko, *ACS Nano*, 2014, **8**, 2360–2368.

29 A. Darwiche, C. Marino, M. T. Sougrati, B. Fraisse, L. Stievano and L. Monconduit, *J. Am. Chem. Soc.*, 2012, **134**, 20805–20811.

30 F. J. Fernández-Madrigal, P. Lavela, C. P. Vicente, J. L. Tirado, J. C. Jumas and J. Olivier-Fourcade, *Chem. Mater.*, 2002, **14**, 2962–2968.

31 L. Aldon, A. Garcia, J. Olivier-Fourcade, J.-C. Jumas, F. J. Fernández-Madrigal, P. Lavela, C. P. Vicente and J. L. Tirado, *J. Power Sources*, 2003, **119–121**, 585–590.

32 P. Ge and M. Fouletier, *Solid State Ionics*, 1988, **28–30**(Part 2), 1172–1175.

33 S. Komaba, Y. Matsuura, T. Ishikawa, N. Yabuuchi, W. Murata and S. Kuze, *Electrochem. Commun.*, 2012, **21**, 65–68.

34 L. Ji, M. Gu, Y. Shao, X. Li, M. H. Engelhard, B. W. Arey, W. Wang, Z. Nie, J. Xiao, C. Wang, J.-G. Zhang and J. Liu, *Adv. Mater.*, 2014, **26**(18), 2901–2908.

35 Y. Xu, Y. Zhu, Y. Liu and C. Wang, *Adv. Energy Mater.*, 2013, **3**, 128–133.

36 Y.-M. Lin, P. R. Abel, A. Gupta, J. B. Goodenough, A. Heller and C. B. Mullins, *ACS Appl. Mater. Interfaces*, 2013, **5**, 8273–8277.